Ionics
https://doi.org/10.1007/s11581-024-05792-y

RESEARCH

Boron-deficient molecules tailored inorganic-rich cathode/electrolyte interfaces for stable Li||$LiFe_{0.2}Mn_{0.8}PO_4$ battery

Guihuang Fang[1,2] · Ying Liu[2] · Ying Pan[2] · Hongwei Yang[1] · Maoxiang Wu[2]

Received: 14 June 2024 / Revised: 24 July 2024 / Accepted: 19 August 2024

Abstract

Tributyl borate (TBB) is among the widely used film-forming electrolyte additives in lithium-ion batteries (LIBs). It possesses the capability to produce an inorganic solid electrolyte interphase with abundant polar boron-containing compounds, functioning as a solid electrolyte interlayer (or cathode electrolyte interlayer), thus effectively isolating the electrode material from the electrolyte and averting parasitic reactions. Herein, the TBB could contribute to the formation of an inorganic solid electrolyte interphase rich in polar B-F and B-O bonds, thus enhancing the stability of the interface between the electrolyte and cathode materials. The findings demonstrate that the inclusion of 0.5 wt% TBB significantly enhances the stability of the electrode/electrolyte interface in Li||$LiMn_{0.8}Fe_{0.2}PO_4$ batteries. After 600 cycles, the specific capacity reaches 107.9 mAh g^{-1} with a capacity retention of 86.45%. This indicates outstanding electrochemical performance and excellent cycling stability. Consequently, TBB exhibits potential as an electrolyte additive for future high-energy density lithium batteries.

Keywords Lithium-ion batteries · TBB · Electrolyte additive · $LiMn_{0.8}Fe_{0.2}PO_4$

Introduction

As electric vehicles, hybrid vehicles, and aerospace sectors advance, the demand for high-performance lithium-ion batteries is on the rise. There is now an urgent requirement for high-energy–density storage solutions to meet future energy storage needs. The olivine-structured lithium transition metal phosphates ($LiMnPO_4$) have been widely investigated and identified as a prospective cathode for high-energy density LIBs due to their higher redox voltage (4.1 V vs Li^+/Li) compared to $LiFePO_4$ (3.4 V vs Li^+/Li) [1–3].

Despite this, the $LiMnPO_4$-based cathode material still experiences capacity degradation during cycling as a result of unfavorable interfacial parasitic reactions between the cathode and the electrolyte [4, 5]. In particular, conventional $LiPF_6$ and ethylene carbonate (EC)-based carbonate electrolytes experience intense oxidative decomposition and dehydrogenation reactions when subjected to voltages exceeding 4.3 V. This process yields by-products such as polycarbonate and $ROCO_2Li$ compounds, accompanied by the generation of CO_x gas and moisture [6]. Moreover, this phenomenon accelerates the decomposition of PF_6^- to produce hydrofluoric acid (HF) and various lithium fluoride compounds ($Li_xPF_yO_z$ and LiF). As a result, it corrodes the transition metal (TM) cations and gives rise to a thick and non-uniform cathode-electrolyte interphase (CEI) layer. the most commonly utilized electrolytes in LIBs consist of $LiPF_6$ salt within mixed EC-based carbonates [7, 8]. In addition, although the oxidation potentials of typical organic solvent-based electrolytes, including EC and DEC, can endure up to 6 V, the presence of transition metals on the cathode surface can result in their oxidation at lower potentials [9, 10]. Hence, to accommodate the aggressive cathodes with higher voltage, the introduction of small quantities of functional

Guihuang Fang and Ying Liu contributed equally to this work.

✉ Guihuang Fang
fang@fjirsm.ac.cn

✉ Hongwei Yang
hongweiy@kust.edu.cn

✉ Maoxiang Wu
mxwu@fjirsm.ac.cn

[1] Faculty of Metallurgy and Energy Engineering, Kunming University of Science and Technology, Kunming 650093, China

[2] Key Laboratory of Optoelectronic Materials Chemistry and Physics, Fujian Institute of Research on the Structure of Matter, Chinese Academy of Sciences, Fuzhou 350002, China

Published online: 26 August 2024

additives into the base electrolyte is considered one of the most economical and effective strategies for enhancing the stability of the interface between the electrolyte and cathode materials [11, 12].

The impact of electrolyte additives on cathode-electrolyte interphase (CEI) and battery performance has been well-demonstrated in the literature [13–15], including numerous boron-based compounds [16–21]. Due to the electron deficiency in the B center atoms, the majority of B-containing additives are capable of forming complexes with anions, thereby stabilizing the carbonate electrolytes. Among these boron-containing additives, including tris(trimethylsilyl) borate (TMSB)[16, 17], trimethyl borate (TB) [18], trimethyl borate (TMB) [19], triethylborate (TEB) [20], and tripropyl borate (TPB) [21], researchers have discovered that these additives can selectively decompose on the delithiated cathode as a result of their higher HOMO energies. This process forms a borate-rich, resilient, and protective interphase, thus enhancing the electrochemical performance of high voltage cathodes. Hence, there is an urgent need to identify suitable electrolyte additives that can physically shield $LiPF_6$ from decomposition without generating any harmful by-products, while also facilitating the formation of an inorganic-rich CEI layer to enhance the stability of the interface between the electrolyte and cathode materials. Recently, several studies have revealed the utilization of TBB in high-voltage cathode materials, such as $LiNi_{0.5}Mn_{1.5}O_4$ (LNMO) [22], $LiNi_{0.6}Mn_{0.2}Co_{0.2}O_2$ [23], and $LiCoO_2$ [24].

To date, the advantageous impact of TBB on high-voltage batteries has primarily been associated with its capacity to create a CEI. In this study, due to the electron deficiency in the B center atom, TBB forms complexes with anions, inhibiting parasitic reactions at the electrode/electrolyte interface that produce HF. This process leads to the development of a solid electrolyte interphase layer rich in inorganic boron, ultimately enhancing the stability of the electrode/electrolyte interface. The results indicate that 0.5 wt% TBB significantly improves the electrode/electrolyte interface stability of Li||$LiMn_{0.8}Fe_{0.2}PO_4$ batteries. After 600 cycles, the specific capacity reaches 107.9 mAh g^{-1} with a capacity retention of 86.45%, which is notably better than the 61.76% exhibited by the base electrolyte, demonstrating outstanding electrochemical performance and excellent cycling stability. Therefore, TBB holds promise as an electrolyte additive for use in next-generation high-energy density lithium batteries.

Experimental

Synthesis of $LiMn_{0.8}Fe_{0.2}PO_4$

$LiMn_{0.8}Fe_{0.2}PO_4$ was synthesized using a modified solid-state method as described elsewhere [3]. Chemicals of LiH_2PO_4, $MnC_4H_6O_4{\cdot}4H_2O$, $FeC_2O_4{\cdot}2H_2O$, and $H_2C_2O_4{\cdot}2H_2O$ with the molar ratio of 1:0.8:0.2:1 were fully ball-milled with sucrose (the molar ratio of sucrose to $MnC_4H_6O_4{\cdot}4H_2O$ was about 0.602) for 6 h, and then the milled mixture was dried and then heated at 700 °C for 15 h under an Ar atmosphere (heating rate: 5 °C min^{-1}).

Preparation of electrolyte and electrode

1.0 M $LiPF_6$-EC/EMC/DMC (ethylene carbonate: ethylmethyl carbonate: dimethyl carbonate of 1:1:1, wt.%) electrolyte was obtained from Dongguan Shanshan Battery Materials Co., Ltd. (China). The electrolyte additive Tributyl borate (TBB, 99%) was purchased from Sigma-Aldrich. Then, 0.5 wt.% TBB was added into the electrolyte in an Ar-filled glove box with ≤ 1 mg L^{-1} water and oxygen. To prepare the $LiMn_{0.8}Fe_{0.2}PO_4$ cathode, $LiMn_{0.8}Fe_{0.2}PO_4$ powder, carbon black (super-P, Alfa), and poly-vinylidene fluoride (PVDF) binder were mixed in N-methylpyrrolidone (NMP) at the weight ratio of 8:1:1 to form a viscous slurry that was cast on aluminum foil and dried at 80 °C for 12 h under vacuum.

Cell assembly

The electrochemical performance of samples was evaluated using the CR2025 coin-type cells with a lithium metal anode. A porous polypropylene (PP) separator (Celgard 2400) with a thickness of 25 μm was placed between the $LiMn_{0.8}Fe_{0.2}PO_4$ cathodes (areal capacity loading of 5.4 mg cm^{-2} and diameter of 14.0 mm) and Li sheets (thickness of 250 μm and diameter of 15.6 mm), and then the electrolytes with and without TBB were used for each cell. Additionally, Al foil was incorporated inside the $LiMn_{0.8}Fe_{0.2}PO_4$ cathode cases to prevent corrosion of the stainless steel case under high voltages. Before cell assembly, the cathodes and separators were thoroughly dried at 80 °C for 12 h under vacuum. All cells were assembled inside a dry glove box that was filled with high-purity argon gas (99.999%) to ensure an inert atmosphere during the assembly process.

Electrochemical measurements

The cells were charged in a constant current-constant voltage (CC-CV) mode and discharged at a constant current using a battery test system (LAND CT2001A, Lanhe Co., Ltd., Wuhan, China). Electrochemical impedance spectroscopy (EIS) was carried out on an electrochemical workstation (VSP, Bio-Logic SAS, France) in a frequency ranged from 100 kHz to 0.01 Hz at 10 mV amplitude. Long-term cycling performance of Li metal was evaluated in Li||Li symmetric cells at a current density of 0.5 mA cm^{-2} for 0.5 mAh cm^{-2}. In the lithium-metal battery configuration (LMBs),

$LiMn_{0.8}Fe_{0.2}PO_4$ was utilized as the cathode and Li sheets at a current density of 1C.

DFT calculations

Theoretical calculations were conducted using Gaussian 16 and density functional theory (DFT) to study the solvents and additive in the electrolyte. The B3LYP/6–311 + + G(d) level was employed for structure and frequency calculations. To examine the solvent effect, the polarized continuum model with acetone (dielectric constant = 20.5) was utilized. After structure optimization, the molecular orbital theoretical calculation values of the molecules (including the solvents and electrolyte additive) as well as the molecular electrostatic potential distribution were obtained.

Measurements

The cells were disassembled in the Ar-filled glove box to analyze the composition and microstructure of the cycled electrodes. All electrodes were cleansed at least five times with DEC to eliminate any residual carbonate solvents and lithium salt and then dried under vacuum for 12 h at room temperature. The crystalline phases of cathodes were determined using X-ray powder diffraction (XRD, Bruker AXS D8-Advance, Germany) employing a Cu Kα source. Data collection was conducted across the 2θ range of 10 − 70°at a scan rate of $0.5°s^{-1}$. Fourier transform infrared adsorption spectroscopy was measured on a NICOLET iS10 spectrometer (FTIR, Thermo Fisher Scientific, USA) using transmittance mode within a range of 400–4000 cm^{-1}. Surface analysis of the electrodes was investigated by X-ray photoelectron spectroscopy (XPS, ESCALAB 250Xi, Thermo Fisher Scientific, USA) using a monochromatic Al Kα source (1486.68 eV). Detailed survey spectra were collected at a pass energy of 20.0 eV, and the data were calibrated using adventitious C 1 s peak with a fixed value of 284.8 eV.

Results and discussion

The molecular orbital theoretical calculation values of the solvent molecules EC, EMC, DMC, and the TBB additive are depicted in Fig. 1 a and b. According to density functional theory (DFT) calculations, the highest occupied molecular orbital (HOMO) energy level of the TBB additive (− 6.91 eV) is significantly lower than that of EC (− 8.93 eV), DMC (− 8.46 eV), and EMC (− 8.73 eV) (Fig. 1b). This indicates that during the charging process, TBB will undergo oxidation decomposition at the surface of the $LiMn_{0.8}Fe_{0.2}PO_4$ cathode before EC, DMC, and EMC solvents. This suggests that TBB can serve as a film-forming additive for the cathode of lithium-ion batteries, inhibiting the oxidative decomposition of the electrolyte during cycling.

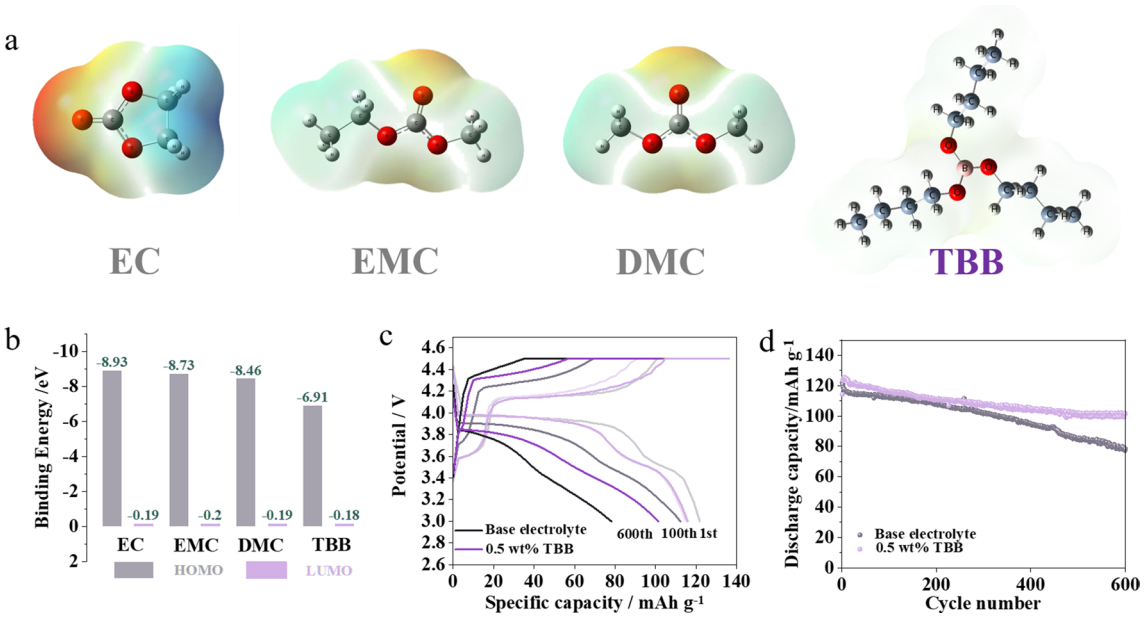

Fig. 1 **a** Molecular electrostatic potential (MESP) distribution of DMC, EMC, EC, and TBB. **b** Highest occupied molecular orbital (HOMO) and lowest unoccupied molecular orbital (LUMO) energy levels of various components in the electrolyte. **c** The typical charge/discharge curves of the $LiMn_{0.8}Fe_{0.2}PO_4$ cathodes cycled at 1 C. **d** Cycle performance at 1 C within the voltage range of 3.0–4.5 V (*vs.* $Li.^+/Li$)

Figure 1c depicts the typical charge–discharge curves of Li||$LiMn_{0.8}Fe_{0.2}PO_4$ cells at different cycles during charge/discharge at 1 C (1 C equals 150 mA g^{-1}) in both the base and the TBB-containing electrolyte. All curves display a similar pattern, featuring two voltage plateaus at approximately 3.5 and 4.1 V, corresponding to the redox couples of Fe^{3+}/Fe^{2+} and Mn^{3+}/Mn^{2+}, respectively. Upon closer observation, it is apparent that compared to the base electrolyte, the initial charge–discharge curve of $LiMn_{0.8}Fe_{0.2}PO_4$ in the TBB electrolyte exhibits higher polarization and lower reversible capacity. This may be due to the increased initial viscosity of the electrolyte resulting from the introduction of TBB, consequently reducing the ion conductivity and wettability of the electrolyte [25]. However, after cycling, there is a shift in this trend, leading to a reduction in polarization within the TBB-containing electrolyte. During the 100th and 600th cycles, it was observed that the polarization induced by the TBB electrolyte was significantly lower than that of the base electrolyte. Particularly in the 600th cycle within the base electrolyte, severe polarization occurred, substantially limiting the reversible capacity of the $LiMn_{0.8}Fe_{0.2}PO_4$ cells during charging. In sharp contrast, in cycles employing the TBB electrolyte, the cells displayed a slower growth of charge–discharge polarization and a higher capacity retention. This trend is also apparent in the electrochemical performance of the $LiMn_{0.8}Fe_{0.2}PO_4$ cells, as illustrated in Fig. 1c. Illustrated in Fig. 1b is the performance cycle of the $LiMn_{0.8}Fe_{0.2}PO_4$ cathode. Notably, the inclusion of TBB in the electrolyte vastly enhances the cycle performance. Following 600 cycles at 1C (where 1C equals 150 mAh g^{-1}), the discharge capacity of the $LiMn_{0.8}Fe_{0.2}PO_4$ cathode demonstrates a decrease from 126.6 to 78.2 mAh g^{-1} in the absence of TBB, maintaining a capacity retention of 61.76%. Conversely, in the presence of TBB, the discharge capacity decreases from 124.8 to 107.9 mAh g^{-1} with a significantly improved capacity retention of 86.45%. These findings underscore how the introduction of TBB into the electrolyte effectively mitigates capacity degradation in the $LiMn_{0.8}Fe_{0.2}PO_4$ cathode during long term cycling.

In order to gain deeper insights into the electrochemical behavior of the $LiMn_{0.8}Fe_{0.2}PO_4$ cathodes cycled in these two electrolytes, electrochemical impedance spectroscopy (EIS) was used, with their resulting spectra recorded at the fully discharged state depicted in Fig. 2 (all cells used for EIS analysis were in a fully discharged state). The EIS spectra commonly display arcs in the high to medium-frequency range, reflecting interfacial impedances such as cathode surface film resistance (Rf) and charge transfer resistance (Rct). Additionally, a sloped line is observed in the low-frequency range, corresponding to Warburg impedance. Furthermore, a sloped line is evident in the low-frequency region, indicative of the Warburg impedance [26]. A noteworthy observation from Fig. 2a is the higher interfacial resistance of the uncycled $LiMn_{0.8}Fe_{0.2}PO_4$ cathode in the TBB-containing

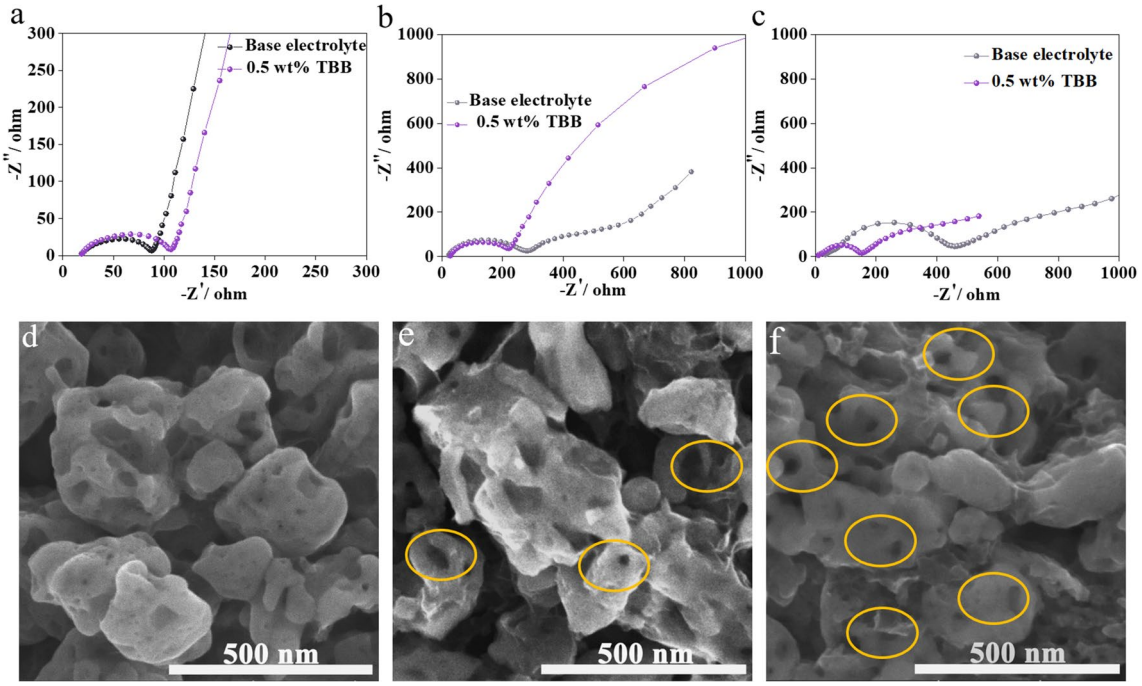

Fig. 2 **a** EIS spectra of the $LiMn_{0.8}Fe_{0.2}PO_4$ cathodes in the base and containing TBB electrolyte recorded at the fully discharge state: (a) uncycled, (b) after 5 cycles, and (c) after 600 cycles **b** SEM images of the $LiMn_{0.8}Fe_{0.2}PO_4$ cathodes: (a) uncycled, (b) after 600 cycles in the base electrolyte, and (c) after 600 cycles in the containing TBB electrolyte

electrolyte as compared to that in the base electrolyte. This observation is consistent with the higher charge/discharge polarization observed during the initial charge/discharge in the TBB-containing electrolyte (Fig. 1c), suggesting that the interaction between the $LiMn_{0.8}Fe_{0.2}PO_4$ cathode and the electrolyte has already begun before cycling, indicating the onset of the TBB's impact. However, after 5 cycles at 0.1 C, the opposite trend is depicted in Fig. 2b, where the interfacial resistances Rf and Rct in the base electrolyte significantly increase, surpassing the resistance observed in the TBB-containing electrolyte. Subsequently, the interfacial resistance in the base electrolyte gradually reaches nearly 2000 Ω after 600 cycles, surpassing the resistance (< 600 Ω) observed in the TBB-containing electrolyte (Fig. 2c). It is clear that the incorporation of TBB into the electrolyte markedly enhances the $LiMn_{0.8}Fe_{0.2}PO_4$ cathode/electrolyte interface, effectively mitigating the increase in interfacial resistance during long-term cycling, thereby facilitating charge transfer at the interface and improving charge/discharge and cycling performance (Fig. 1c,d).

The EIS findings suggest that interfacial parasitic reactions between the $LiMn_{0.8}Fe_{0.2}PO_4$ cathode and the electrolyte result in the formation of a solid interfacial film (SEI) on the cathode surface throughout cycling. To authenticate the existence of this interfacial film, scanning electron microscopy (SEM) were utilized. The SEM images in Fig. 2d–f depict the uncycled $LiMn_{0.8}Fe_{0.2}PO_4$ cathode, as well as the cathodes after 600 cycles in electrolytes both base and TBB-containing electrolyte. In contrast to the porous nature of the uncycled $LiMn_{0.8}Fe_{0.2}PO_4$ particles and their open pores (Fig. 2d), it is evident that the pores inside the particles of the cathode cycled in the base electrolyte are significantly obstructed (Fig. 2e), while the extent of pore blockage is notably reduced in the TBB-containing electrolyte (Fig. 2f). This provides direct evidence of the presence of an interfacial film on the surface of the $LiMn_{0.8}Fe_{0.2}PO_4$ cathode, indicating that more products resulting from interfacial parasitic reactions were created on the cathode cycled in the base electrolyte (Fig. 2e). The pore blockage on the cathode surface will hinder the penetration of the electrolyte and the extraction/insertion of Li^+ among the $LiMn_{0.8}Fe_{0.2}PO_4$ particles, ultimately leading to heightened charge/discharge polarization. Given the above findings, it can be inferred that the incorporation of TBB in the electrolyte effectively inhibits interfacial parasitic reactions and enhances the $LiMn_{0.8}Fe_{0.2}PO_4$ cathode/electrolyte interface. This results in the formation of a thinner interfacial film and fewer blocked pores in the TBB-containing electrolyte, ultimately improving the electrochemical performance of the $LiMn_{0.8}Fe_{0.2}PO_4$.

To explore the compounds deposited due to interfacial parasitic reactions between the $LiMn_{0.8}Fe_{0.2}PO_4$ cathode and the electrolyte during cycling, the cathodes after 600 cycles were retrieved and analyzed through XPS, XRD, and FTIR measurements. Figure 3a illustrates the XRD patterns of the pristine Li $Mn_{0.8}Fe_{0.2}PO_4$ cathode and those subsequent to 600 cycles in both base and TBB-containing electrolytes. Alongside multiple peaks originating from the current collector, specifically the graphite-coated aluminum foil, a marginal alteration is detected in the diffraction peaks of the $LiMn_{0.8}Fe_{0.2}PO_4$ following 600 cycles in the base electrolyte. Moreover, two additional diffraction peaks appearing around $2\theta = 18$ and 31 (marked by *) are observed in the XRD pattern of the cathode cycled in the base electrolyte. While exact assignments are challenging to ensure, it is reasonable to attribute the peaks (indicated by *) to the $Mn_{0.8}Fe_{0.2}PO_4$ delithiated phase [27]. The absence of these two diffraction peaks in the XRD pattern of the cathode cycled in the TBB-containing electrolyte may suggest a reduced loss of Li^+ from the $LiMn_{0.8}Fe_{0.2}PO_4$ cathode following 600 cycles in the TBB-containing electrolyte. In order to further analyze the chemical composition of the cathode interface, I utilized FTIR analysis technologies.

As depicted in Fig. 3b, $Mn_{0.8}Fe_{0.2}PO_4$ delithiation phase is evident around 1264, 1082, 1036, 990, 956, and 942 cm^{-1} for both base and TBB-containing cathodes [28, 29], validating the depletion of Li^+ after 1000 cycles and the creation of $Mn_{0.8}Fe_{0.2}PO_4$ which corroborates the findings from XRD analysis (Fig. 3a). Significantly, additional peaks appear in the spectra of the two cycled cathodes in comparison to the uncycled cathode. These include LiF (775 cm^{-1}), Li_xPF_y (842 cm^{-1}), Li_2CO_3 (1520 − 1450 and 878 cm^{-1}), $Li_xPO_yF_z$ (1080 cm^{-1}), and polycarbonate (1805 and 1775 cm^{-1}), representing the distinct peaks of the compounds resulting from interfacial parasitic reactions between the cathode and the electrolyte [30]. Due to the shielding effect of these deposited products on the cathode surface, the intensity of peaks associated with PO_4^{3-} (1137, 1096, 1049, 962, 641, 582, and 546 cm^{-1}) is reduced [27, 28]. Notably, the intensity of the PO_4^{3-} peaks varies between the cathodes cycled in the two electrolytes, potentially linked to the diverse fractions of these compounds arising from the cathode/electrolyte interfacial parasitic reactions.

The compounds resulting from the interfacial side reactions between the $LiMn_{0.8}Fe_{0.2}PO_4$ cathode and the electrolyte during cycling were additionally examined via XPS, as depicted in Fig. 3c–i. In the C 1 s spectrum of the cycled cathode, the peak at 284.8 eV corresponds to C − C bonds present in the graphite phase [31], while the peaks at 286.0, 288.7, 290.0, and 290.8 eV can be attributed to the C − O, C = O, Li_2CO_3, and C − F bonds within the PVDF, respectively (Fig. 3c) [31]. The intensity of the Li_2CO_3 peak in the C 1 s spectrum of the cathode cycled in the TBB-containing electrolyte is observed to be lower compared to that in the base electrolyte, indicating reduced Li_2CO_3 production in the TBB-containing electrolyte during cycling. A similar

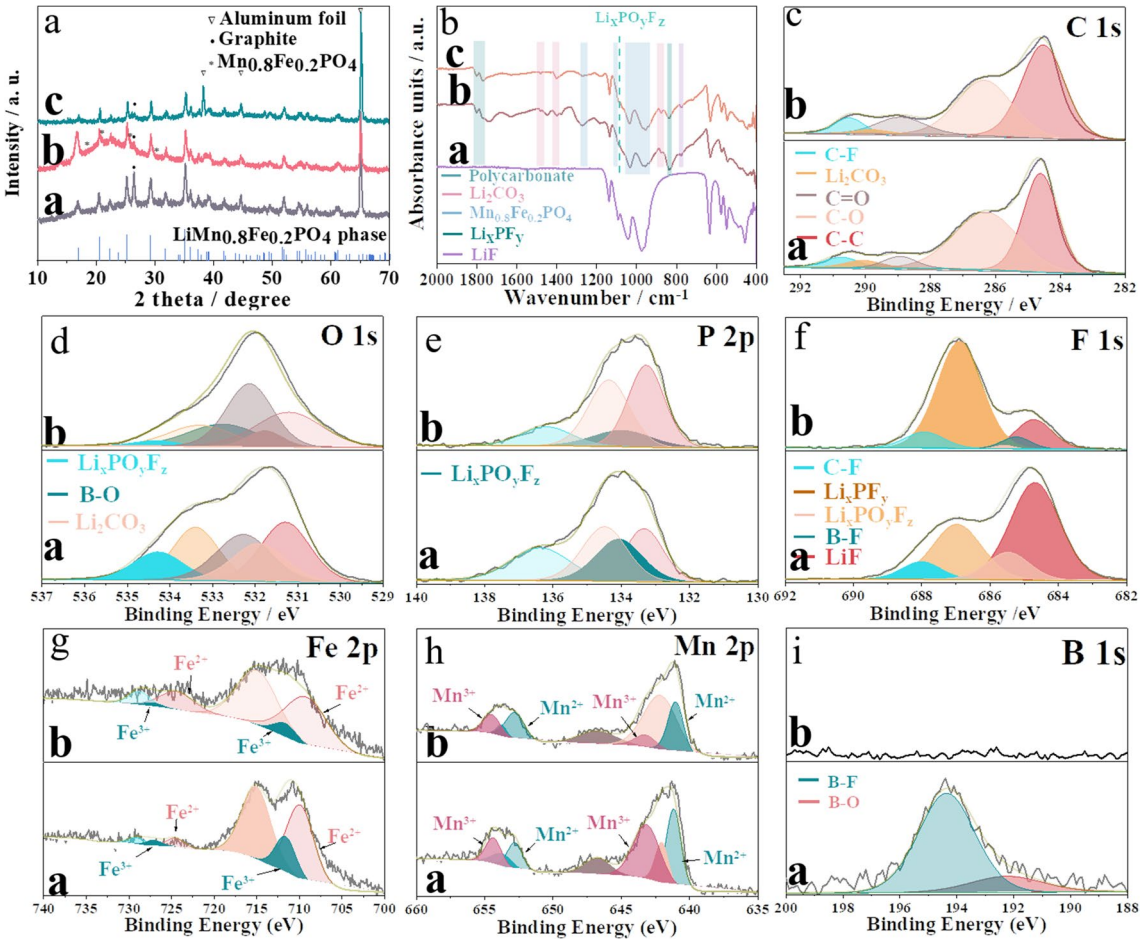

Fig. 3 The XPS spectra of $LiMn_{0.8}Fe_{0.2}PO_4$ cathodes: **a** 600 cycles in the electrolyte without additive and **b** 600 cycles in the electrolyte containing TBB electrolyte

trend is also reflected in the O 1 s spectra, where the Li_2CO_3 peak at 531.5 eV exhibits reduced intensity in the spectrum of the cathode cycled in the TBB-containing electrolyte (Fig. 3d) [31]. Obviously, the $Li_xPO_yF_z$ peak in the cathode cycled in the TBB-containing electrolyte is notably weaker compared to that in the base electrolyte, suggesting a lower generation of $Li_xPO_yF_z$ in the TBB-containing electrolyte during cycling [32, 33]. The existence of $Li_xPO_yF_z$ is further substantiated by the P 2p spectrum, as indicated by a peak at 134.0 eV (Fig. 3e) [31]. Additionally, the F 1 s spectra confirm the existence of $Li_xPO_yF_z$ with a peak at 685.8 eV (Fig. 3f) [31]. Likewise, the intensity of the $Li_xPO_yF_z$ peak in both the P 2p and F 1 s spectra notably diminishes for the cathode cycled in the TBB-containing electrolyte compared to that in the base electrolyte (Fig. 3 e and f).

Furthermore, within the F 1 s spectra of the cycled cathodes, a newly identified peak corresponding to LiF emerges at 684.8 eV (Fig. 3f) [34, 35], with the intensity of this LiF peak notably reduced for the cathode cycled in the TBB-containing electrolyte. It is widely accepted that increased intensity of LiF peaks corresponds to higher battery impedance, attributed to the low ion conductivity of LiF. This phenomenon may account for the lower interfacial resistance observed in cathode cycled with TBB-containing electrolyte (Fig. 2c), in comparison to the base electrolyte. Apparently, the presence of interfacial parasitic reaction products on the cycled cathode surface, including Li_2CO_3, polycarbonate, LiF, and $Li_xPO_yF_z$, is affirmed by the C 1 s, O 1 s, P 2p, and F 1 s spectra of the cycled $LiMn_{0.8}Fe_{0.2}PO_4$ cathodes, which corroborates the findings from FTIR analysis (Fig. 3b). Furthermore, the reduced peak intensity of these products offers evidence supporting the effective mitigation of interfacial parasitic reactions between the $LiMn_{0.8}Fe_{0.2}PO_4$ cathode and electrolyte through the addition of TBB in the electrolyte. Additionally, the Mn 2p and Fe 2p spectra exhibit the existence of Mn^{3+} (peaks at 642 and 654.5 eV) and Fe^{3+} species (peaks at 712.5 and 726 eV) in the cycled cathodes (Fig. 3g,h) [36], consistent with the identification of the $Mn_{0.8}Fe_{0.2}PO_4$ delithiation phase on the previously observed cycled $LiMn_{0.8}Fe_{0.2}PO_4$ cathodes via FTIR and

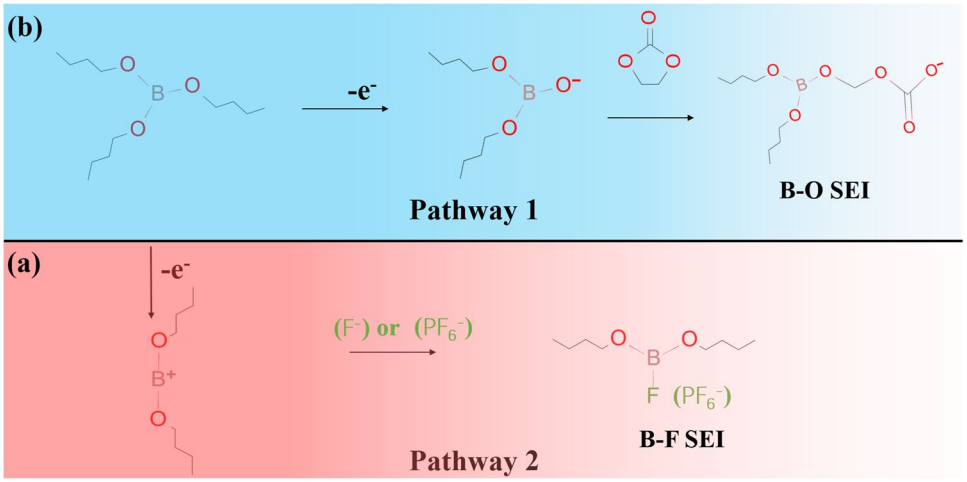

Fig. 4 Possible mechanism of oxidation of TBB

XRD analysis (Fig. 3a,b), indicating the depletion of active Li^+ from the cathode and the initiation of irreversible reactions during extended cycling. Evidently, the heightened intensity of Mn^{3+} and Fe^{3+} peaks in the cathode cycled in the base electrolyte, in comparison to that in the TBB-containing electrolyte, indicates a larger formation of Mn^{3+} and Fe^{3+}-containing compounds within the $LiMn_{0.8}Fe_{0.2}PO_4$ cathode cycled using the base electrolyte. The heightened presence of these compounds indicates a more substantial depletion of active Li^+, leading to accelerated capacity degradation and shortened 4.1 and 3.5 V charge – discharge plateaus for the $LiMn_{0.8}Fe_{0.2}PO_4$ cathode cycled in the base electrolyte (Fig. 1c,d), which collectively have a detrimental effect on the overall electrochemical performance of the cell. All these findings validate the effective mitigation of electrolyte component decomposition, encompassing solvents and $LiPF_6$, through the utilization of TBB.

In the B 1 s XPS spectra for $LiMn_{0.8}Fe_{0.2}PO_4$ cathode cycled in the TBB-containing electrolyte (Fig. 3i), only two faint peaks are detected: one at 192.5 eV, representing B-O containing species, and the other at 194.0 eV for the B-F bond [22–24]. These findings provide confirmation that TBB contributes to the formation of the interphase on $LiMn_{0.8}Fe_{0.2}PO_4$. The bond energy of B-O exceeded that of C-O, resulting in a tendency for C-O to break [23]. Nevertheless, TBB, being an electron-deficient boron compound, readily reacts with electron-rich groups such as PF_6^- and F^-. We have put forward potential pathways for the degradation of TBB, illustrated in Fig. 4 [23, 24]. TBB ($C_{12}H_{27}BO_3$) undergoes preferential oxidation, resulting in the generation of $(C_8H_{18}BO_2)^+$ and $C_4H_9^+$ ions as well as $C_8H_{18}BO_3\bullet$ and $C_4H_9O\bullet$ radicals (Fig. 4). The electron-deficient nature of the boron element in TBB results in its affinity to combine with the electron-rich groups (i.e., as PF_6^- and F^-). Meanwhile, the abundance of anions surrounding TBB causes the intermediate state $(C_8H_{18}BO_2)^+$ formed during the oxidation of TBB to preferentially interact with anions, leading to the formation of B-F species (Fig. 4a). Moreover, the $C_8H_{18}BO_3\bullet$ radical interacts with EC to form B-O based species (Fig. 4b). Through strong binding with anions, TBB reduces the association of protons and anions, thereby decreasing HF generation and effectively inhibiting the consumption of active Li^+ in the cathode as well as subsequent electrolyte decomposition. Simultaneously, TBB, together with the electrolyte, establishes an inorganic positive electrode interphase rich in B-O and B-F, ultimately significantly enhancing the cycling stability of $LiMn_{0.8}Fe_{0.2}PO_4$.

Conclusions

Improved surface properties of the $LiMn_{0.8}Fe_{0.2}PO_4$ cathode material were attained through the utilization of TBB as a highly effective functional additive. Due to the electron deficiency in the B center atom, TBB forms complexes with anions (PF_6^- and F^-), thereby inhibiting parasitic reactions that generate HF at the electrode/electrolyte interface, fostering the development of a solid electrolyte interphase rich in inorganic boron, and ultimately enhancing the stability of the electrode/electrolyte interface. The findings reveal that incorporating 0.5 wt% TBB significantly enhances the stability of the electrode/electrolyte interface in $Li||LiMn_{0.8}Fe_{0.2}PO_4$ batteries. After 600 cycles, the specific capacity reaches 107.9 mAh g^{-1}, with a capacity retention of 86.45%, exhibited by the base electrolyte. These results demonstrate outstanding electrochemical performance and remarkable cycling stability. Therefore, TBB exhibits potential as an electrolyte additive for next-generation high-energy density lithium batteries.

Author contribution Guihuang Fang: Conceptualization, Data curation, Methodology, Validation, Visualization, Writing – original draft, Writing – review & editing. Ying Liu: Conceptualization, Data curation,

Formal analysis, Validation. Ying Pan: Writing – original draft, Writing – review & editing. Hongwei Yang: Data curation, Formal analysis, Software, Visualization. Maoxiang Wu: Conceptualization, Funding acquisition, Project administration, Resources, Supervision, Writing – review & editing.

Funding This work is supported by the National Natural Science Foundation of China (grant numbers 12275274).

Data availability No datasets were generated or analysed during the current study.

Declarations

Conflict of interest The authors declare no competing interests.

References

1. Aravindan V, Gnanaraj J, Lee YS (2013) $LiMnPO_4$-a next generation cathode material for lithium-ion batteries. J Mater Chem A 1:3518–3539
2. Chung SY, Bloking JT, Ching YM (2003) On the electronic conductivity of phospho-olivines as lithium storage electrodes. Nat Mater 2:702–703
3. Chen W, Luo QY, Fang HS (2022) Ameliorated Li^+ extraction/insertion kinetics and stability of $LiMnPO_4$ by Al^{3+} doping. Phy Chem Chem Phy 24:28599–28608
4. Chen W, Fang HS (2024) Lattice modulation improving surface passivation of $LiMnPO_4$ for stable cycling at high temperatures. Prog Solid State Chem 74:100460
5. Fang HS, Dai ER, Yang B (2012) $LiMn_{0.8}Fe_{0.19}Mg_{0.01}PO_4$/C as a high performance cathode material for lithium ion batteries. J Power Sources 204:193–196
6. Zhao JT, Zhang X, Liang Y, Han ZJ, Yu HJ (2021) Interphase engineering by electrolyte additives for lithium-rich layered oxides: advances and perspectives. ACS Energy Lett 6:2552–2564
7. Chu X, Chen W, Fang HS (2021) Hydrothermal synthesis of olivine phosphates in the presence of excess phosphorus: a case study of $LiMn_{0.8}Fe_{0.19}Mg_{0.01}PO_4$. Ionics 27:3259–3269
8. Han JG, Kim K, Lee Y, Choi NS (2019) Scavenging materials to stabilize $LiPF_6$-containing carbonate-based electrolytes for Li-Ion batteries. Adv Mater 31:1804822
9. Li LM, Lu XP, Chen W, Fang HS (2019) A new strategy to hydrothermally synthesize olivine phosphates. Chem Commun 55:12092
10. Moskon J, Pivko M, Jerman I (2016) Cycling stability and degradation mechanism of $LiMnPO_4$ based electrodes. J Power Sources 303:97–108
11. Amine K, Liu J, Belharouak I (2005) High-temperature storage and cycling of C-$LiFePO_4$/graphite Li-ion cells. Electrochem Commun 7:669–673
12. Wang J, Zhao DN, Cong YY, Cui XL (2021) Analyzing the mechanism of functional groups in phosphate additives on the interface of $LiNi_{0.8}Co_{0.15}Al_{0.05}O_2$ cathode materials. ACS Appl Mater Interfaces 13:16939–116951
13 Fang GH, Chen W, Fang HS (2024) Improved performance of $LiMn_{0.8}Fe_{0.2}PO_4$ by addition of fluoroethylene carbonate electrolyte additive. Chin Chem Lette 35:108799
14 Wei C, Liu Y, Yu C (2024) SnF_2-induced multifunctional interface-stabilized $Li_{5.5}PS_{4.5}Cl_{1.5}$-based all-solid-state lithium metal batteries. Adv Funct Mater 34:2314306
15. Fang GH, Pan Y, Yang HW (2024) Enhanced $LiMn_{0.8}Fe_{0.2}PO_4$ cathode performance enabled by the 1,3,2-dioxathiolane-2,2-dioxide electrolyte additive. J Phys Chem C. https://doi.org/10.1021/acs.jpcc.4c00459
16. Wang J, Dong H, Wang P, Fu XL, Li SY, Cui XL (2022) Adjusting the solvation structure with tris(trimethylsilyl)borate additive to improve the performance of LNCM half cells. J Energy Chem 67:55–64
17. Cui XL, Zhu JL, Wang J, Li SY (2024) Enhancing compatibility between $LiNi_{0.8}Co_{0.1}Mn_{0.1}O_2$ and $LiPF_6$-based electrolyte via bis(trimethylsilyl)oxalate additive. Mater Today Energy 43:101573
18. Wang Z, Xing L, Li J (2015) Trimethyl borate as an electrolyte additive for high potential layered cathode with concurrent improvement of rate capability and cyclic stability. Electrochim Acta 184:40–46
19. Li J, Xing L, Hang L (2016) Insight into self-discharge of layered Lithium-rich oxide cathode in carbonate-based electrolytes with and without additive. J Power Sources 324:17–25
20. Wang Z, Xing L, Li J (2016) Triethylborate as an electrolyte additive for high voltage layered lithium nickel cobalt manganese oxide cathode of lithium ion battery. J Power Sources 307:587–592
21. Li J, Xing L, Wang Z (2018) Insight into the capacity fading of layered lithium rich oxides and its suppression via a film-forming electrolyte additive. RSC Adv 8:25794–25801
22. Huang T, Zheng XZ, Wu MX (2019) The effect of tributyl borate on electrochemical performance at an elevated temperature of high-voltage $LiNi_{0.5}Mn_{1.5}O_4$ cathode. ACS Appl Mater & Inter 11:26873–26879
23. Li JH, Yang XR, Guan XC, Fan WZ, Li WS (2019) Efficiently suppressing oxygen evolution in high voltage graphite/NCM pouch cell with tributyl borate as electrolyte additive. Electrochim Acta 354:136722
24 Qin ZM, Hong B, Duan BY (2018) Tributyl borate as a novel electrolyte additive to improve high voltage stability of lithium cobalt oxide in carbonate-based electrolyte. Electrochim Acta 276:412–416
25. Wu BB, Pei F, Wu Y (2013) An electrochemically compatible and flame-retardant electrolyte additive for safe lithium ion batteries. J Power Sources 227:106–110
26 Li YC, Wan S, Veith GM (2017) A novel electrolyte salt additive for lithium ion batteries with voltages greater than 4.7 V. Adv Energy Mater 7:1601397
27. Chu X, Li LM, Chen W, Fang HS (2021) Hydrothermal synthesis and electrochemical performance of multicomponent $LiMn_{0.8}Fe_{0.19}Mg_{0.01}PO_4$. Ionics 27:2927–2935
28. Burba CM, Frech R (2004) Raman and FTIR spectroscopic study of Li_xFePO_4 ($0 \le x \le 1$). J Electrochem Soc 151:A1032–A1038
29. Norberg NS, Kostecki R (2011) FTIR spectroscopy of a $LiMnPO_4$ composite cathode. Electrochim Acta 56:9168–9171
30. Aurbach D, Gnanaraj JS, Geissler W, Schmidt M (2004) Vinylene carbonate and Li salicylatoborate as additives in $LiPF_3(CF_2CF_3)_3$ solutions for rechargeable Li-ion batteries. J Electrochem Soc 151:A23
31. Lu DS, Xu MQ, Zhou L (2013) Failure mechanism of graphite/$LiNi_{0.5}Mn_{1.5}O_4$ cells at high voltage and elevated temperature. J Electrochem Soc 160:A3138–A3143
32. Andersson AM, Edstro MK (2001) Chemical composition and morphology of the elevated temperature SEI on graphite. J Electrochem Soc 148:A1100
33. Ensling D, Stjerndahl M, Nyten A (2009) A comparative XPS surface study of Li_2FeSiO_4/C cycled with LiTFSI- and $LiPF_6$-based electrolytes. J Mater Chem 19:82–88
34. Aurbach D, Gamolsky K, Markovsky B (2000) The study of surface phenomena related to electrochemical lithium intercalation

into Li_xMO_y host materials (M = Ni, Mn). J Electrochem Soc 147:1322
35. Kim K, Kim Y, Oh ES (2013) The role of fluoride in protecting $LiNi_{0.5}Mn_{1.5}O_4$ electrodes against high temperature degradation. Electrochim Acta 114:387–393
36. Gueguen A, Castro L, Dedryvered R (2013) The electrode/electrolyte reactivity of $LiFe_{0.33}Mn_{0.67}PO_4$ compared to $LiFePO_4$. J Electrochem Soc 160:A387–A393